

Preconditioned implicit PDE solvers for degenerate parabolic equations with applications to monument conservation

Matteo Semplice, Marco Donatelli, Stefano Serra-Capizzano *

December 10, 2018

Abstract

We are interested in the mathematical models for the description, in a quantitative way, of the damages induced on the monuments by the action of specific pollutants. A quantitative knowledge of such a degradation is of great importance in precise scheduling of cleaning or deeper restoration works. The analytical study of the solution of the considered models has been conducted and validated by the group of Natalini in Rome. The latter reveals important and partly unexpected features of the time evolution of the damages, but only in an asymptotic sense, that is for large times. However, for a short window of time, we need to couple such a study with a numerical approximation scheme in order to have a quantitative forecast at any time of interest. The novel contribution of this paper relies in the proposal of a fully implicit numerical method, in its convergence/stability analysis, and in the study of the related computational cost. In fact, due to the nonlinear nature of the underlying mathematical model, the use of a fixed point scheme is required and every step implies the solution of large, locally structured, linear systems. A special effort is devoted to the spectral analysis of the relevant matrices and to the design of appropriate iterative or multi-iterative solvers, with special attention to preconditioned Krylov methods and to multigrid procedures. Numerical experiments for the validation of our multi-facet analysis complement this contribution.

1 Introduction

The problem of monitoring, preserving and, when needed, restoring monuments and works of art has become more and more relevant in recent years for the conservation of our cultural heritage, after the recognition of the negative effects of some pollutants on the monuments. Numerous studies made researchers

*Dipartimento di Fisica e Matematica, Università dell'Insubria - Sede di Como, Via Valleggio 11, 22100 Como, Italy, **E-mail:** {matteo.semplice, marco.donatelli, stefano.serrac}@uninsubria.it

and restorers more and more aware that gaseous pollutants, atmospheric particulate matter, and some microorganisms can adversely affect the status of our monuments. In order to monitor the cultural heritage and for precisely programming the restoration works, it is of paramount importance to be able to accurately assess the status of each monument. Along these lines, quantitative methods are emerging and making their way into the practice of preservation and restoration. These have the obvious advantage of allowing fair comparison of the state of different monuments, supporting the decision process on what to restore, clean, etc and on the relative urgency of each case.

As an example, consider the “black crusts” that grow on marble surfaces as an effect of sulfation of the carbonate stone that is turned into gypsum when reacting with SO_2 in a moist environment. Since urban concentration can be nowadays more than 100 times higher than the atmospheric basal values, this effect has become very important in the last decades. Sulfation can cause permanent damage to the monuments because gypsum crusts can be easily eroded by rain or (when located in protected areas) can become unaesthetically black including particulate matter from the atmosphere and eventually exfoliate [Hay83, GKAC89, BLTR00].

A better scheduling of cleaning or deeper restoration can be devised if the thickness (and composition) of the crust can be forecast in quantitative way, providing a way to compute and thus predict the time evolution of the crust. The most common quantitative evaluation of the sulfation phenomena that is used in practice consists in assuming that the thickness is directly proportional to the length of time of the exposure to the pollutants, with a proportionality coefficient obtained by fitting data from a large number of monuments [Lip89]. Although this may give an average indication good enough for civil buildings, the uniqueness and cultural importance of a work of art calls for a more detailed analysis, that can take into account the local environment to which the monument is exposed.

A mathematical model of the sulfation of marble based on the chemical reactions involved was developed by Natalini and coworkers [ADDN04, GN05] at IAC-CNR (Rome) and tested against experiments in collaboration with ICR (Istituto Centrale del Restauro) and CISTeC (Centro di Ricerca in Scienza e Tecnica per la Conservazione del Patrimonio Storico-Architettonico - Roma La Sapienza) [GSNF08].

It is worthwhile to remark that the mathematical model is able to provide new information, which partly contradicts the most common quantitative evaluation methods based on data fitting. In particular (see [GN07]) the asymptotic study of the equations in a one dimensional setting reveals that for large times the thickness of the gypsum crust does not grow proportionally to the elapsed time as in the Lipfert formula, but proportionally to its square root: the speed of growth of the crust is significantly reduced as time goes on. Clearly this means that a complete removal of the crust will speed up the damage and calls for study of optimal strategies for the periodic partial crust removal.

However the asymptotic analysis does not give enough information on what happens for short times and moreover the study is not yet available for complex

geometries. For example on a corner stone, SO_2 penetrates the marble from two sides: how does the crust grow? Does it get rounded? How much? And, more importantly, what about the fine particulars of decorations or statues? In some cases sulfation caused an almost complete loss of details: can the model predict the thickness of the crust there and allow the scheduling of an optimal conservation strategy? In order to answer the previous questions, we need a numerical method to solve the equations of the model developed by the group in Rome (see [ADDN04]). This is a system of two equations, one of which is nonlinear of parabolic type.

In this paper we study novel numerical techniques to integrate for long times nonlinear, possibly degenerate, parabolic equations like those appearing in the model by [ADDN04]. We wish to point out that the techniques developed here have applications that go beyond the aforementioned model. For example, in the area of conservation, they could be adapted to numerically investigate the more complete sulfation model described in [AFNT07] and the consolidation model presented in [CGN⁺].

Indeed the ambition of our interdisciplinary research group (Co.MoNum¹) at Insubria University, Science Faculty of Como, is to pursue this line of research and in particular to study and validate experimentally mathematical models relevant for the novel approach of *planned conservation*, also furnishing numerical techniques with their complete analysis also for complicate geometries (frequently encountered in real monuments) and to test the models on one or two symbolic monuments in the town of Como in collaboration with the local and national institutions.

As a prototype we first consider a single equation of the form

$$\frac{\partial u}{\partial t} = \frac{\partial}{\partial x} \left(D(u) \frac{\partial u}{\partial x} \right) \quad (1)$$

where $D(u)$ is non-negative function and the equation is called degenerate whenever $D(u)$ vanishes.

In the literature, degenerate parabolic equations have been discretized mainly using explicit or semi-implicit methods, thus avoiding to solve the nonlinear equation arising from the elliptic operator. A remarkable class of methods arise directly from the so-called non-linear Chernoff formula [BP72] for time advancement, coupling it with a spatial discretization: for finite differences this was started in [BBR79] and for finite elements by [MNV87]. More recently, another class related to the relaxation approximation emerged: such numerical procedures exploit high order non-oscillatory methods typical of the discretization of conservation laws and their convergence can be proved making use of semigroup arguments similar to those relevant for proving the Chernoff formula [CNPS07].

In this paper instead we start from the Crandall-Liggett formula

$$U(t^n, x) - \Delta t L_D(U(t^n, x)) = U(t^{n-1}, x), \quad (2)$$

¹Co.MoNum is composed by M. Donatelli (Numerical Analysis), F. Ferri (Physics of material and optics), N. Ossanna-Cavadini (Architecture), L. Rampazzi (Analytical Chemistry), M. Semplice (Applied Mathematics and Numerical Analysis), S. Serra Capizzano (Numerical Analysis)

where time has been discretized and $\Delta t = t^n - t^{n-1}$ and $-L_{D(\cdot)}$ denotes the elliptic operator $u \mapsto -(D(u)u_x)_x$. The computation of $U(t^n, x)$ now requires to solve a nonlinear equation whose form is determined by the elliptic operator and the nonlinear function $D(u)$, but the convergence is guaranteed without restrictions on the time step Δt [CL71]. Furthermore, due to the nonlinear nature of the underlying mathematical model, the use of a fixed point scheme is required and the choice of the faster Newton-like methods implies the solution at every step of large, locally structured (in the sense of Tilli, see [T98]) linear systems. A special effort is devoted to the spectral analysis of the relevant matrices and to the design of appropriate iterative or multi-iterative solvers [S93], with special attention to preconditioned Krylov methods and to multigrid procedures (see [G97, Sa96, H85, TOS01] and references therein for a general treatment of iterative solvers). Numerical experiments for the validation of our multi-facet analysis complement this contribution.

The paper is organized as follows. In Section 2 we couple the time discretization (2) with a spatial discretization based on finite differences and set up a Newton method for the resulting system of nonlinear equations. In Section 3 we report the explicit form of the Jacobian appearing in the Newton iterations and consider various algorithms of multi-iterative type for the solution of the involved linear systems. A brief spectral analysis of the related matrix structures is provided in order to give an appropriate motivation for the good behavior of the proposed iterative or multi-iterative solvers. In Section 4 we perform some numerical tests, while in 5 we apply the techniques to the case of the sulfation model by [ADDN04]. A conclusion section with a short plan for future investigations completes the paper.

2 Numerical methods for the PDE

In order to discretize equations like (1), we will employ a time semidiscretization given by the Crandall-Liggett formula and a space discretization based on finite differences, explained in the following subsection. The latter numerical choice leads to a system of coupled nonlinear equations that needs to be solved at each discrete timestep in order to compute the solution of the PDE: this is achieved using the Newton method, as detailed in Subsection 2.2. The scheme is summarized in Subsection 2.3, where we also report and comment convergence results.

2.1 Finite difference discretization

We take into consideration a standard discretization in space using finite differences. In the interval $[a, b]$ we take $N+1$ points with equal spacing $h = (b-a)/N$ $x_k = a + kh$ and we denote by U_k^n the approximate solution at time t^n and location x_k . Furthermore \vec{U}^n is the vector of size N containing the collection of the values U_k^n , $k = 1, \dots, N$, on the whole grid at time t^n . When no confusion

As already observed $L_{D(\vec{v})}$ is a symmetric real tridiagonal matrix. If $D(\cdot)$ is a nonnegative function then, by the first Gerschgorin Theorem (see e.g. [GV83]), the matrix $-L_{D(\vec{v})}$ is always positive semidefinite, since the matrix is weakly diagonally dominant by row. Furthermore, we have positive definiteness (i.e. invertibility), at least for every N large enough, if in addition $\phi(\cdot)$ has only isolated zeros in (a, b) . In that case the matrix is irreducible or block diagonal with irreducible blocks. For that it is enough that D has only isolated zeros. Finally in the case where $\phi(\cdot)$ is strictly positive in (a, b) then $-L_{D(\vec{v})}$ is positive definite and irreducible.

More sophisticated relations will be discussed later when choosing the appropriate iterative solvers for the global linearized system; see Subsection 3.1. For the moment we just observe that, thank to the previous preliminary spectral analysis, all the classical iterative solvers like Jacobi and Gauss-Seidel (and their damped version with damping parameter belonging to $(0, 2)$) are all convergent for the solution of a linear system with such a coefficient matrix. The problem is that the spectral radii are very close to 1, with a gap ranging between $O(N^{-2})$, reached by all these classical iterations with the only exception of the optimally damped Gauss-Seidel, and $O(N^{-1})$, reached for Gauss-Seidel with optimal damping parameter; see [V62]. When considering the whole system things become slightly better since the gap between the spectral radius and 1 reduces for all the considered procedures to $O(N^{-1})$. However, as a partial conclusion, we can safely claim the considered iterations would be unacceptably slow and the search for specialized iterative solvers becomes mandatory. The latter is the main subject of Section 3.

2.2 The nonlinear system and the Newton iteration

Following the Crandall-Liggett formula (2), in order to compute \vec{U}^n from \vec{U}^{n-1} , we need to solve the nonlinear vector equation

$$\vec{U}^n = \vec{U}^{n-1} + \frac{\Delta t}{h^2} L_{D(\vec{U}^n)} \vec{U}^n$$

where, as already mentioned, the vector \vec{U}^n denotes the collection of the values U_k^n , $k = 1, \dots, N$, on the whole grid at time t^n . We set up Newton iterations for the vector function

$$F(\vec{U}) = \vec{U} - \frac{\Delta t}{h^2} L_{D(\vec{U})} \vec{U} - \vec{U}^{n-1}. \quad (5)$$

In order to understand the convergence of the Newton scheme, it is crucial to have an expression for the Jacobian of $F(\vec{U})$. We report the generic partial

derivative that is

$$\begin{aligned} \frac{\partial F_k}{\partial U_j} &= \delta_{jk} - \frac{\Delta t}{h^2} L_{D(U)}|_{j,k} - \frac{\Delta t}{2h^2} \left[\begin{array}{l} (D'_{k-1}\delta_{k-1,j} + D'_k\delta_{k,j}) U_{k-1} - \\ - (D'_{k-1}\delta_{k-1,j} + 2D'_k\delta_{k,j} + D'_{k+1}\delta_{k+1,j}) U_k + \\ + (D'_k\delta_{k,j} + D'_{k+1}\delta_{k+1,j}) U_{k+1} \end{array} \right] \\ &= \delta_{jk} - \frac{\Delta t}{h^2} L_{D(U)}|_{j,k} - \frac{\Delta t}{2h^2} \left[\begin{array}{l} \delta_{k-1,j} D'_{k-1} (U_{k-1} - U_k) + \\ + \delta_{k,j} D'_k (U_{k-1} - 2U_k + U_{k+1}) + \\ + \delta_{k+1,j} D'_{k+1} (U_{k+1} - U_k) \end{array} \right]. \quad (6) \end{aligned}$$

The first two terms $X_N(\cdot) = I_N - \Delta t/h^2 L_{D(\cdot)}$ form a symmetric positive definite matrix with eigenvalues ≥ 1 (strictly greater under assumption of isolated zeros). The third term $Y_N(\cdot)$ is the product of a diagonal matrix with entries D'_k and a tridiagonal matrix $\text{tridiag}_k[U_{k-1} - U_k, U_{k-1} - 2U_k + U_{k+1}, U_{k+1} - U_k]$. The latter matrix is not symmetric and can be symmetrized, which implies a real spectrum, if the diagonal matrix is positive semidefinite. The latter amounts in requiring that $D(\cdot)$ is a smooth nondecreasing function. In any case it can be easily observed that $Y_N(\cdot)$ shows an infinitesimal spectral norm in the case where the values U_k , $k = 0, \dots, N$, represent the approximation with infinitesimal error of a continuous function over the used uniform grid. In that case the spectral norm is bounded from above by a universal constant times the maximum between the approximation error to the analytic solution and the modulus of continuity of the solution evaluated at N^{-1} . Hence, since we are using second order formulae, the error is dominated by the modulus of continuity of the solution at N^{-1} , which is of order exactly equal N^{-1} , if the solution is Lipschitz continuous. In conclusion we can safely claim that the global spectrum of the Jacobian is decided, up to small perturbations, by the matrix $X_N(\cdot)$.

2.3 The scheme

Denote $\vec{U}^{n,s}$ the s^{th} Newton iterate for the computation of \vec{U}^n and by $\|\cdot\|$ the standard Euclidean norm (and its induced matrix norm). The jacobian matrix of $F(U)$ is denoted by $F'(U) = \left[\frac{\partial F_k}{\partial U_j} \right]_{j,k=1}^N$. The scheme can be summarized as follows

1. Initialize \vec{U}^0 with the initial value $U_k^0 = u_0(x_k)$.
2. For each timestep $n \geq 1$

- (a) Set $\vec{U}^{n,0} = \vec{U}^{n-1}$
- (b) Repeat

$$\vec{U}^{n,s+1} = \vec{U}^{n,s} - \left[F'(\vec{U}^{n,s}) \right]^{-1} F(\vec{U}^{n,s}) \quad (7)$$

until $\|\vec{U}^{n,s+1} - \vec{U}^{n,s}\| / \|\vec{U}^{n,s}\| < \varepsilon = c \cdot h$

- (c) Set $\vec{U}^n = \vec{U}^{n,s+1}$

3. Stop when final time of simulation is reached

Since the Crandall-Liggett formula does not induce any restriction on the timestep Δt [CL71], we have only to prove the convergence of the Newton method (7). We are interested in the choice $\Delta t = Ch$ for a constant C independent of h , which gives a method which is overall first order convergent. This is no restriction due to the presence of singularities at degenerate points: higher order methods would be more computationally intensive without reaching their convergence rate.

Indeed, concerning the stopping criterion the following observation is of interest. Since the method is of first order in time Δt can be chosen equal to h , it is sufficient to set $\varepsilon = c \cdot h$ where c is moderately small constant independent of h . In fact, more precision will be useless in practice and would make the Newton process more expensive by increasing the iteration count. The following result is a classical tool (see [OR70]) for handling the global convergence of the Newton procedure.

Theorem 2.1 (Kantorovich). *Consider the Newton method (7) with $\vec{U}^{n,0} = \vec{U}^{n-1}$. Under the assumption that*

$$\| [F'(\vec{U}^{n-1})]^{-1} \| \leq \beta, \quad (8a)$$

$$\| [F'(\vec{U}^{n-1})]^{-1} F(\vec{U}^{n-1}) \| \leq \eta, \quad (8b)$$

$$\| F'(\vec{U}) - F'(\vec{V}) \| \leq \gamma \| \vec{U} - \vec{V} \|, \quad (8c)$$

and that

$$\beta\eta\gamma < \frac{1}{2}, \quad (9)$$

we find that the Newton iteration is convergent and, in addition, the stationary point of the iterations lies in the ball with center \vec{U}^{n-1} and radius

$$\frac{1 - \sqrt{1 - 2\beta\eta\gamma}}{\beta\gamma}.$$

For the choice $\Delta t = Ch$ we can prove the following result.

Proposition 2.2. *The Newton method (7) is convergent when initialized with the solution at the previous timestep (i.e. $\vec{U}^{n,0} = \vec{U}^{n-1}$) and for $\Delta t \leq Ch$.*

Proof. We will make use of the Kantorovich Theorem 2.1, so we need to estimate (8) and to show that relation in (9) is satisfied. We will use the Euclidean vector norm and the induced matrix norm (spectral norm), and, for the sake of notational simplicity, we set $A = F'(\vec{U}^{n-1})$.

For estimating the (8a), first of all we show that $\frac{A+A^T}{2}$ is positive definite. The symmetric part of $F'(\vec{U}^{n-1})$ is

$$\frac{A + A^T}{2} = I - \frac{\Delta t}{h^2} L_{D(\vec{U}^{n-1})} - \frac{\Delta t}{2h^2} \text{tridiag}_k \begin{bmatrix} (D'_k - D'_{k-1})(U_{k-1} - U_k) \\ D'_k(U_{k-1} - 2U_k + U_{k+1}) \\ (D'_{k+1} - D'_k)(U_{k+1} - U_k) \end{bmatrix},$$

which is positive definite because the third term, the only with indefinite symmetric part, is in fact negligible compared with the remaining part under our assumption that $\Delta t = h$ and by assuming $D(\cdot)$ and the solution smooth enough. In fact, under the above hypotheses, we have that every entry of the third term is of order $\frac{\Delta t}{2h^2}h^2$ that is $O(h)$ and since the matrix is banded also the spectral norm is of the same order. We now notice that

$$\|A^{-1}\|_2 = \frac{1}{\sigma_{\min}(A)} \leq \lambda_{\min}\left(\frac{A + A^T}{2}\right)^{-1},$$

where we denotes by $\sigma_{\min}(\cdot)$ and $\lambda_{\min}(\cdot)$ the minimum singular value and the minimum eigenvalue of the argument, respectively. Clearly for the latter inequality we have to show that

$$\sigma_{\min}(A) \geq \lambda_{\min}\left(\frac{A + A^T}{2}\right). \quad (10)$$

We make use of the auxiliary matrix

$$B = \begin{bmatrix} 0 & A^T \\ A & 0 \end{bmatrix}$$

which is symmetric and with eigenvalues $\lambda_1(B) = \sigma_1(A) \geq \dots \geq \lambda_n(B) = \sigma_n(A) \geq \lambda_{n+1}(B) = -\sigma_n(A) \geq \dots \geq \lambda_{2n}(B) = -\sigma_1(A)$, since the Schur decomposition of B is easily written in terms of the singular value decomposition of A (see [Bh97, GV83]). Let \mathcal{V} be a vector space and $\vec{x} \in \mathbb{R}^n$ such that $\|\vec{x}\|_2 > 0$. We obtain

$$\begin{aligned} \sigma_{\min}(A) &= \sigma_n(A) = \lambda_n(B) \\ &= \max_{\dim(\mathcal{V})=n} \min_{\vec{y} \in \mathcal{V}} \frac{\vec{y}^T B \vec{y}}{\vec{y}^T \vec{y}} \geq \min_{\vec{y} = [\vec{x}^T \ \vec{x}^T]^T} \frac{\vec{y}^T B \vec{y}}{\vec{y}^T \vec{y}} = \min_{\vec{x} \in \mathbb{R}^n} \frac{\vec{x}^T (A^T + A) \vec{x}}{2\vec{x}^T \vec{x}} \\ &= \lambda_{\min}\left(\frac{A + A^T}{2}\right). \end{aligned}$$

Moreover $\lambda_{\min}\left(I - \frac{\Delta t}{h^2}L_D(\vec{U}^{n-1})\right) \geq 1$ and the spectral norm of

$$\frac{\Delta t}{2h^2} \text{tridiag}_k \begin{bmatrix} (D'_k - D'_{k-1})(U_{k-1} - U_k) \\ D'_k(U_{k-1} - 2U_k + U_{k+1}) \\ (D'_{k+1} - D'_k)(U_{k+1} - U_k) \end{bmatrix}$$

is $O(\Delta t)$ so that

$$\lambda_{\min}\left(\frac{A + A^T}{2}\right) \geq 1 - O(\Delta t). \quad (11)$$

Hence

$$\beta \leq 1 + O(\Delta t), \quad (12)$$

where the constant hidden in the big O contains the infinity norms of the first and second derivatives of the solution and the infinity norm of the second derivative of $D(\cdot)$.

For (8b) observe that \vec{U}^{n-1} is the stationary point of the Newton iteration for the previous time step and thus it satisfies

$$\vec{U}^{n-1} + \frac{\Delta t}{h^2} L_{D(\vec{U}^{n-1})} \vec{U}^{n-1} = \vec{U}^{n-2}.$$

Hence

$$\| [F'(\vec{U}^{n-1})]^{-1} F(\vec{U}^{n-1}) \| \leq \beta \| F(\vec{U}^{n-1}) \| = \beta \| \vec{U}^{n-2} - \vec{U}^{n-1} \| \leq \beta C_1 \Delta t$$

for a constant C_1 independent of h . It follows that

$$\eta = C_1 \beta \Delta t. \quad (13)$$

For the Lipschitz constant of F' , i.e., for estimating (8c), observe that $F'(\vec{U}) - F'(\vec{V})$ is a tridiagonal matrix with two contributions:

$$F'(\vec{U}) - F'(\vec{V}) = \frac{\Delta t}{h^2} (L_{D(\vec{U})} - L_{D(\vec{V})}) - (Y_N(\vec{U}) - Y_N(\vec{V})), \quad (14)$$

where $Y_N(\cdot)$ denotes the last term in (6). The first can be estimated as follows:

$$\| L_{D(\vec{U})} - L_{D(\vec{V})} \|_2 \leq \| L_{D(\vec{U})} - L_{D(\vec{V})} \|_\infty \leq 4 \| D' \|_\infty \| \vec{U} - \vec{V} \|_\infty. \quad (15)$$

In order to check that the last inequality holds, one observes that the sum of the absolute values of the elements in each row of $L_{D(\vec{U})} - L_{D(\vec{V})}$ is smaller than the sum of 4 terms of the form

$$\begin{aligned} \left| D_{k\pm 1/2}(\vec{U}) - D_{k\pm 1/2}(\vec{V}) \right| &= \left| D \left(\frac{U_{k\pm 1} + U_k}{2} \right) - D \left(\frac{V_{k\pm 1} + V_k}{2} \right) \right| \\ &= |D'(\zeta)| \frac{|U_{k\pm 1} + U_k - V_{k\pm 1} - V_k|}{2} \leq \| D' \|_\infty \| \vec{U} - \vec{V} \|_\infty. \end{aligned}$$

For the second term in (14), we have

$$\| Y_N(\vec{U}) - Y_N(\vec{V}) \|_2 \leq \frac{\Delta t}{2h^2} \| D' \|_\infty \| M \|_2, \quad (16)$$

where

$$M = \text{tridiag}_k \begin{bmatrix} (U_{k-1} - U_k) - (V_{k-1} - V_k) \\ (U_{k-1} - 2U_k + U_{k+1}) - (V_{k-1} - 2V_k + V_{k+1}) \\ (U_{k+1} - U_k) - (V_{k+1} - V_k) \end{bmatrix}$$

and

$$\| M \|_2 \leq \left\| \frac{M + M^T}{2} \right\|_2 + \left\| \frac{M - M^T}{2} \right\|_2 \leq 3 \| \vec{U} - \vec{V} \|_\infty. \quad (17)$$

Replacing equation (17) in (16) and combining (16) and (15) with (14), we obtain

$$\gamma \leq \frac{11}{2} \|D'\|_\infty \frac{\Delta t}{h^2}, \quad (18)$$

because $\|\vec{U} - \vec{V}\|_\infty \leq \|\vec{U} - \vec{V}\|_2$.

Finally, combining equations (12), (13), and (18), Theorem 2.1 implies that Newton converges provided that

$$\frac{1}{2} \geq \beta\eta\gamma = C_1 \frac{11}{2} \|D'\|_\infty \frac{(\Delta t)^2}{h^2} \beta^2,$$

i.e., $\Delta t \leq Ch$, up to lower order terms, for $C = 1/\sqrt{11C_1\|D'\|_\infty}$ (essentially) independent on h . \square

The proof technique used for bounding from below the minimal singular value of a the matrix A is part of a more general framework useful for refining, when necessary, the estimates. In fact, in general it can be proved that for any complex-valued matrix A the minimal singular value is not less than the distance d_r of any straight line r separating the numerical range of A from the complex zero. Therefore a better estimate can be obtained by making the sup that we call d of d_r , for all straight lines that induce the separation. In our case we used the fact that the real part of A (that is $\text{Re}(A) = (A + A^*)/2$) is positive definite and so our straight line becomes the set of all complex numbers having real part equal to $\lambda_{\min}(\text{Re}(A))$. The estimate could be poor since the latter straight line is not necessarily tangent to the numerical range (a convex set by the Toeplitz-Hausdorff theorem, see [Bh97]): thus d could be much larger than d_r . However in our setting such an estimate is already very satisfactory, as also stressed by the numerical experiments.

3 Algorithms for the resulting linear systems

At each Newton iteration, we need to solve a linear system whose coefficient matrix is represented by the Jacobian $F'(\vec{U})$ with entries as in (6). In principle, the Jacobian is recomputed at each Newton iteration, so we are interested in efficient iterative methods for solving the related linear system.

We note in passing that the form of the Jacobian matrix used here is very similar to the one that is obtained discretizing in space with P_1 conforming finite elements. Thus the methods considered here can be to some extent generalized to finite elements approximations. In particular, when considering real $2D$ and $3D$ cases, the structure of the relevant matrices will depend heavily on the geometry of the domain, on the triangulation/gridding (often generated automatically), and on the type of finite elements (higher order or non Lagrangian etc.). Therefore fast methods that are based on a rigid algebraic structure (e.g. of Toeplitz type) cannot be adapted because the structure is lost, in the considered general framework. However there exists a kind of information

depending only on the continuous operator and which are inherited virtually unchanged in both finite differences and finite elements, provided that the grids are quasi-uniform in finite differences and the angles are not degenerating in finite elements. Such information consists in the spectral features (conditioning, subspaces related to small eigenvalues etc.) and these spectral features are conveniently used when defining ad hoc preconditioned Krylov methods or multigrid algorithms, working uniformly well in one or more dimensions. More specifically, we will consider the following choices.

- GMRES without preconditioning and with symmetric preconditioner given by $P_N(\cdot) = I_N - \Delta t/h^2 L_{D(\cdot)}$ to be handled by a standard V-cycle (basic multigrid with damped Jacobi as smoother).
- Conjugate gradient (CG) without preconditioning and with symmetric preconditioner given by $P_N(\cdot) = I_N - \Delta t/h^2 L_{D(\cdot)}$ to be handled again by a standard V-cycle (basic multigrid with damped Jacobi as smoother)
- Multigrid (MGM) with V-cycle structure and basic damped Jacobi as smoother. For comparison, we will also consider pre and post smoothing to be chosen by varying into the classical iterative solvers and looking, as much as possible, at the spectral complementarity in the spirit of multi-iterative solvers [S93].
- Krylov techniques with few V-cycle iterations as preconditioning step: this would represent a computationally less expensive version of the first two suggestions. In particular the number of V-cycle iterations could be taken fixed e.g. at one iterations or adjusted step by step as a function of the current precision. In [ST04] it was shown that this strategy is sometimes very effective for reducing the number of iterations without affecting the linear cost per iteration of the V-cycle procedure.

3.1 Spectral analysis for the resulting matrix-sequences

We start by introducing the notion of spectral distribution for a matrix sequence. Then we will briefly report a concise analysis of some delicate spectral features of the matrices involved in the definition of the Jacobian. Since the emphasis of this work relies in the computational aspects and in the verification of the goodness of the model, we will not report all possible details, nuances, and generalizations of the spectral analysis.

Definition 3.1. *Let $\mathcal{C}_0(\mathbb{R}_0^+)$ be the set of continuous functions with bounded support defined over the nonnegative real numbers, d a positive integer, and θ a complex-valued measurable function defined on a set $G \subset \mathbb{R}^d$ of finite and positive Lebesgue measure $\mu(G)$. Here G will be often equal to $(-\pi, \pi)^d$ so that $e^{i\overline{G}} = \mathbb{T}^d$ with \mathbb{T} denoting the complex unit circle. A matrix sequence $\{A_N\}$ is said to be distributed (in the sense of the singular values) as the pair (θ, G) ,*

or to have the distribution function θ ($\{A_N\} \sim_\sigma (\theta, G)$), if, $\forall F \in \mathcal{C}_0(\mathbb{R}_0^+)$, the following limit relation holds

$$\lim_{N \rightarrow \infty} \frac{1}{N} \sum_{j=1}^N F(\sigma_j(A_N)) = \frac{1}{\mu(G)} \int_G F(|\theta(t)|) dt, \quad t = (t_1, \dots, t_d). \quad (19)$$

Furthermore, a matrix sequence $\{A_N\}$ is said to be distributed (in the sense of the eigenvalues) as the pair (θ, G) , or to have the eigenvalue distribution function θ ($\{A_N\} \sim_\lambda (\theta, G)$), if, $\forall F \in \mathcal{C}_0(\mathbb{C})$, the following limit relation holds

$$\lim_{N \rightarrow \infty} \frac{1}{N} \sum_{j=1}^N F(\lambda_j(A_N)) = \frac{1}{\mu(G)} \int_G F(\theta(t)) dt, \quad t = (t_1, \dots, t_d). \quad (20)$$

Along with the distribution in the sense of singular values/eigenvalues (weak*-convergence), for the practical convergence analysis of iterative solvers we are also interested in a further asymptotic property called here the *clustering*.

Definition 3.2. A matrix sequence $\{A_N\}$ is strongly clustered at $s \in \mathbb{C}$ (in the eigenvalue sense), if for any $\epsilon > 0$ the number of the eigenvalues of A_n off the disk

$$D(s, \epsilon) := \{z : |z - s| < \epsilon\}$$

can be bounded by a pure constant q_ϵ possibly depending on ϵ , but not on n . In other words

$$q_\epsilon(n, s) := \#\{\lambda_j(A_N) : \lambda_j \notin D(s, \epsilon)\} = O(1), \quad n \rightarrow \infty.$$

If every A_N has only real eigenvalues (at least for all n large enough), then s is real and the disk $D(s, \epsilon)$ reduces to the interval $(s - \epsilon, s + \epsilon)$. Furthermore, $\{A_N\}$ is strongly clustered at a nonempty closed set $S \subset \mathbb{C}$ (in the eigenvalue sense) if for any $\epsilon > 0$

$$q_\epsilon(n, S) := \#\{\lambda_j(A_N) : \lambda_j \notin D(S, \epsilon) := \cup_{s \in S} D(s, \epsilon)\} = O(1), \quad n \rightarrow \infty, \quad (21)$$

$D(S, \epsilon)$ is the ϵ -neighborhood of S , and if every A_N has only real eigenvalues, then S has to be a nonempty closed subset of \mathbb{R} . Finally, the term “strongly” is replaced by “weakly”, if

$$q_\epsilon(n, s) = o(n), \quad (q_\epsilon(n, S) = o(n)), \quad n \rightarrow \infty,$$

in the case of a point s (a closed set S), respectively. The extension of the notion in the singular value sense is trivial and is not reported in detail.

It is clear that $\{A_N\} \sim_\lambda (\theta, G)$ ($\{A_N\} \sim_\sigma (\theta, G)$) with $\theta \equiv s$ a constant function is equivalent to $\{A_n\}$ being weakly clustered in the eigenvalues sense at $s \in \mathbb{C}$ (in the singular value sense at $s \in \mathbb{R}_0^+$).

Now we briefly use the above concepts in our specific setting. Indeed, taking into account $\Delta t = h$ and the rescaling, our sequence $\{A_N\}$ is formed in the following way:

$$\begin{aligned} A_N &= -L_{D(\vec{U})} + hI_N + \text{tridiag}_k \begin{bmatrix} U_{k-1} - U_k \\ U_{k-1} - 2U_k + U_{k+1} \\ U_{k+1} - U_k \end{bmatrix} \text{diag}_k [D'_k] \\ &= -L_{D(\vec{U})} + hI_N + Y_N(\vec{U}). \end{aligned}$$

We have the following results, which are of crucial interest in the choice, in the design, and in the analysis of efficient solvers for the involved linear systems.

- The conditioning in spectral norm of A_N is of order N : this is implied directly by the verification of condition (8a) that is inequality (12) in Theorem 2.1.
- By using the Bendixson Theorem the eigenvalues of A_N are localized in a rectangle having real part in $[ch, D]$ and imaginary part in $[-dh, dh]$ for some positive constants c, d, D independent of N : this statement is again implied by the analysis provided in Theorem 2.1.
- $\{A_N\} \sim_{\lambda, \sigma} (\theta, G)$ with $\theta(x, s) = D(u(x))(2 - 2\cos(s))$, $G = [a, b] \times [0, 2\pi]$ (distribution of the zero order main term). The distribution of $\{L_{D(\vec{U})}\}$ is already known (see [T98]), if we assume that \vec{U} is a sampling of a given function over a uniform grid. In our case the entries of \vec{U} represent an approximation in infinity norm of the true solution, the latter being implied by the convergence of the method, and therefore by standard perturbation arguments we deduce $\{L_{D(\vec{U})}\} \sim_{\lambda, \sigma} (\theta, G)$ with θ and G as above. Moreover the trace norm (sum of all singular values i.e. Schatten p norm with $p = 1$; see [Bh97]) of the remaining part $hI_N + Y_N(\vec{U})$ is bounded by a pure constant C independent of N , when assuming that $D'(\cdot)$ is bounded and $u(\cdot)$ is at least Lipschitz continuous. The latter implies that the distribution of $\{A_N\}$ is decided only by the symmetric part that is, essentially, $\{L_{D(\vec{U})}\}$; see Theorem 3.4 in [GS07]. Moreover any real interval containing the spectrum $\{L_{D(\vec{U})}\}$ is also a strong eigenvalue clustering set for $\{A_N\}$; see Corollary 3.3 and Theorem 3.5 in [GS07].
- $\{hI_N + Y_N(\vec{U})\} \sim_{\lambda, \sigma} (0, G)$ and $\{I_N + Y_N(\vec{U})/h\} \sim_{\lambda, \sigma} (\theta, G)$ with $\theta(x, s) = 1 + D'(u(x))2i\sin(s)$, $G = [a, b] \times [0, 2\pi]$ (distribution of the first order term): the analysis is of the same type as in the previous item.
- Setting $P_N = -L_{D(\vec{U})} + hI_N$, we have $\{P_N^{-1}A_N\} \sim_{\lambda, \sigma} (0, G)$ (equivalent, as already observed, to a weak eigenvalue/singular value clustering): it follows from the property of algebra of the Generalized Locally Toeplitz (GLT) sequences; see [S02].

- In fact the preconditioned sequence $\{P_N^{-1}A_N\}$ is also strongly clustered at zero both in the eigenvalue and singular value sense: we remark that the strong clustering property can be recovered via local domain analysis, by employing the same tools and the same procedure as in Theorem 3.7 of [BGST05] (see also Section 3.1 and the conclusion section in [BS07] and references therein).

The last property is very important in practice, since it is crucial for deducing a number of iterations of preconditioned GMRES bounded by a constant depending on the precision, but not on the mesh that is on h (optimality of the method).

3.2 Multi-iterative idea and MGM methods

Let $A \in \mathbb{C}^{n \times n}$ be a matrix with positive definite real part $\text{Re}(A) = (A + A^*)/2$, and let $\vec{b} \in \mathbb{C}^n$, m integer with $0 < m < n$. Fix integers $n_0 = n > n_1 > n_2 > \dots > n_m > 0$, take $P_{i+1}^i \in \mathbb{C}^{n_{i+1} \times n_i}$ full-rank matrices and consider a class \mathcal{R}_i of iterative methods for n_i -dimensional linear systems. The related V-cycle method (see [H85, TOS01]) produces the sequence $\{\vec{x}^{(k)}\}_{k \in \mathbb{N}}$ according to the rule $\vec{x}^{(k+1)} = \text{MGM}(0, \vec{x}^{(k)}, \vec{b})$, with MGM recursively defined as follows:

$$\begin{array}{l} \vec{x}_i^{(\text{out})} := \text{MGM}(i, \vec{x}_i^{(\text{in})}, \vec{b}_i) \\ \hline \text{If } (i = m) \text{ Then Solve}(A_m \vec{x}_m^{(\text{out})} = \vec{b}_m) \\ \text{Else } \begin{array}{l} \mathbf{1} \quad \vec{r}_i := A_i \vec{x}_i^{(\text{in})} - \vec{b}_i \\ \mathbf{2} \quad \vec{b}_{i+1} := P_{i+1}^i \vec{r}_i \\ \mathbf{3} \quad A_{i+1} := P_{i+1}^i A_i (P_{i+1}^i)^H \\ \mathbf{4} \quad \vec{y}_{i+1} := \text{MGM}(i+1, \vec{0}_{n_{i+1}}, \vec{b}_{i+1}) \\ \mathbf{5} \quad \vec{x}_i^{(\text{int})} := \vec{x}_i^{(\text{in})} - (P_{i+1}^i)^H \vec{y}_{i+1} \\ \mathbf{6} \quad \vec{x}_i^{(\text{out})} := \mathcal{R}_i^\nu(\vec{x}_i^{(\text{int})}) \end{array} \end{array} \quad (22)$$

Step 1 calculates the residual of the proposed solution; steps 2, 3, 4, and 5 define the *recursive coarse grid correction*, by projection (step 2) of the residual, sub-grid correction (steps 3, 4), and interpolation (step 5), while step 6 performs some (ν) iterations of a “post-smoother”.

By using the MGM as an iterative technique, at the k -th iteration, we obtain the linear systems $A_i \vec{x}_i^{(k)} = \vec{b}_i^{(k)}$, $i = 0, \dots, m$, where the matrices $A_i \in \mathbb{C}^{n_i \times n_i}$ have all positive definite real part, i.e., $\text{Re}(A_i) > 0$. Only the last is solved exactly while all the others are recursively managed by reduction to low-level system and smoothing. The procedures \mathcal{R}_i are most of the times one-point methods (see [RS87]) with prescribed linear part $R_i \in \mathbb{C}^{n_i \times n_i}$, i.e.,

$$\mathcal{R}_i(\vec{x}_i) = R_i \vec{x}_i + (I_{n_i} - R_i) A_i^{-1} \vec{b}_i^{(k)}, \quad \vec{x}_i \in \mathbb{C}^{n_i}, \quad i = 0, \dots, m-1. \quad (23)$$

If we define the multigrid iteration matrix of level $i = m - 1, \dots, 0$ as MGM_i

$$\begin{cases} MGM_m = O_{n_m \times n_m} \\ MGM_i = R_i^\nu \cdot \left[I_{n_i} - (P_{i+1}^i)^H (I_{n_{i+1}} - MGM_{i+1}) A_{i+1}^{-1} P_{i+1}^i A_i \right], \end{cases} \quad (24)$$

then $\vec{x}_i^{(\text{out})} = MGM_i \vec{x}_i^{(\text{in})} + (I_{n_i} - MGM_i) A_i^{-1} \vec{b}_i$, so in the finer grid we have $\vec{x}^{(k+1)} = MGM_0 \vec{x}^{(k)} + (I_{n_0} - MGM_0) A_0^{-1} \vec{b}$, and MGM_i depends on i but not on any $\vec{x}_i^{(k)}$ neither on $\vec{b}_i^{(k)}$. The algorithm has essentially two degrees of indetermination:

1. choice of the projectors P_{i+1}^i , $i = 0, \dots, m - 1$;
2. choice of the smoothers \mathcal{R}_i , $i = 0, \dots, m - 1$.

The choice of the projectors P_{i+1}^i , and the calculation of the matrices A_i is performed before the beginning of the V-cycle procedure (pre-computing phase).

In many applications also a pre-smoother is used. This amounts in adding a step 0 totally similar to step 6 where a further one-point method is employed. In this way the matrix in (24) has to be multiplied on the right by a further iteration matrix and so

$$MGM_i = R_{i,\text{post}}^{\nu_{i,\text{post}}} \cdot \left[I_{n_i} - (P_{i+1}^i)^H (I_{n_{i+1}} - MGM_{i+1}) A_{i+1}^{-1} P_{i+1}^i A_i \right] R_{i,\text{pre}}^{\nu_{i,\text{pre}}},$$

where we have also considered a number of smoothing steps depending on the level $i = m - 1, \dots, 0$. In practice (see [ADS04, ST04] and references therein) the application of this further iteration accelerates the global convergence substantially and the explanation of this phenomenon falls outside the convergence theory of the algebraic multigrid and indeed pertains to multi-iterative methods [S93].

For instance, looking just at the two-grid method, in the case of the d -dimensional discrete Laplacian, it is easy to prove that the post-smoothing given by the Richardson iteration with $\omega = \omega_1 \equiv \frac{1}{4d}$ is strongly converging in the subspace of the high frequencies that the coarse grid correction strongly reduces the error in the low frequencies subspace. Therefore, if we look at the combination of the two iterations, which separately are slowly convergent on the global space \mathbf{C}^n , we discover that the complementarity leads to a fast convergent two-grid method. However, a finer analysis tells us that the global error is now essentially localized in the middle frequencies: the iteration given again by Richardson but with $\omega = \omega_2 \equiv \frac{1}{2d}$ is not a smoother, but it is fast convergent just in the middle frequencies subspace. Therefore its further use in step 6 or equivalently in step 0 increases very much the “spectral complementarity,” so that we obtain a real multi-iterative method whose spectral radius is really small. We will call an iteration having a spectral behavior complementary to both the coarse grid correction and the smoother an “intermediate iteration.” In this sense the Richardson iteration with $\omega_2 = 2\omega_1$ is an example of an “intermediate iteration” at least in the case of the discrete Laplacian.

Another degree of freedom used in the recent literature (see [ST04]) is a slight modification of the procedure where we allow, in steps 0 and 6, to have a number of smoothing iterations depending on the level i : it can be easily shown that a polynomial growth with i does not affect the global cost, that remains linear for banded structures, only changing the constants involved in the big O . The surprise in our present setting is that the method that achieves the smallest theoretical cost and that minimizes the CPU times, for reaching the solution with a preassigned accuracy ϵ , is the simplest V-cycle with only one step of post-smoothing given by a classical damped Jacobi.

The reason of the observed behavior relies in the spectral features of our linear algebra problem: indeed, the coefficient matrix is not exactly a weighted Laplacian but it can be viewed, after rescaling, as a regularized weighted Laplacian since in the coefficient matrix one adds h times the identity; see the previous subsection. In this way the conditioning is not growing as the square of the size as in the standard one-level Laplacian but grows only linearly with N . Therefore the basic V-cycle, with one single step of damped Jacobi as pre-smoother, not only is already optimal (number of iterations independent of the system size), but the number of iterations for reaching a given accuracy is already very moderate (10, 11 iterations). Therefore the additional cost per iteration, that should be paid for increasing the number of smoothing steps and for the use of a pre-smoother, can not be compensated by a remarkable reduction of the iteration count.

4 Numerical tests

In this section we consider as a test case the porous medium equation written in the form

$$\frac{\partial u}{\partial t} = \frac{\partial}{\partial x} \left(mu^{m-1} \frac{\partial u}{\partial x} \right) \quad (25)$$

with homogeneous Dirichlet boundary conditions. Here $m \geq 1$, with $m = 1$ corresponding to the heat equation. In particular we consider the exact self-similar solution

$$u(t, x) = t^{-\alpha} \left[1 - k (|x|t^{-\alpha})^2 \right]_+^{\frac{1}{m-1}} \quad \alpha = 1/(m+1), \quad k = \alpha \frac{m-1}{2m} \quad (26)$$

due to Barenblatt and Pattle (The subscript $+$ denotes the positive part). We preliminary remark that increasing m , the loss of regularity at the corner discontinuity, makes numerical approximations harder.

4.1 Convergence of the global method and of Newton's method

First we check the convergence of the method. We perform test for m ranging from 2 to 5, observing no appreciable difference in the convergence properties of the algorithm. In all tests we choose $\Delta t = h$.

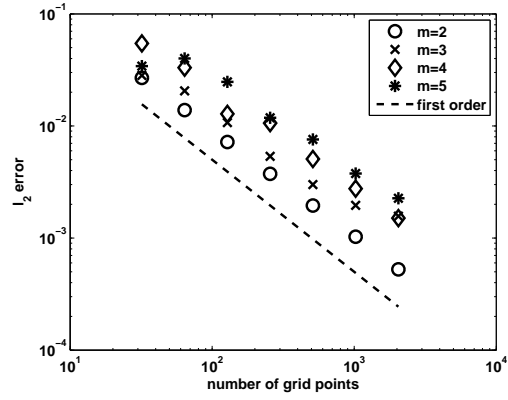


Figure 1: l_2 error at final time for $N = 32, 64, \dots, 2048$, $m = 2$, final time $t = 20/32$, $\Delta t = h$.

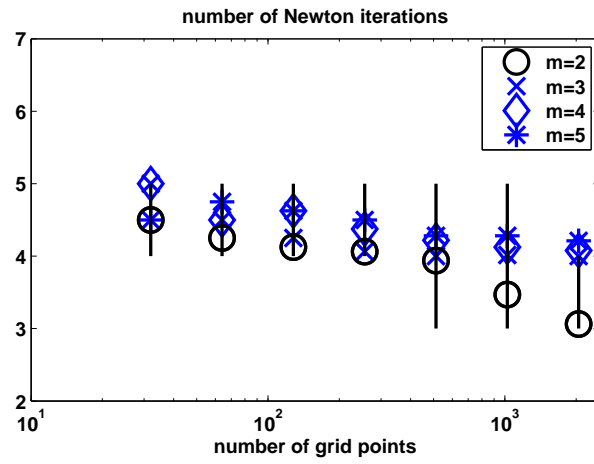


Figure 2: Average, minimum and maximum number of Newton iterations performed during the integration until final time.

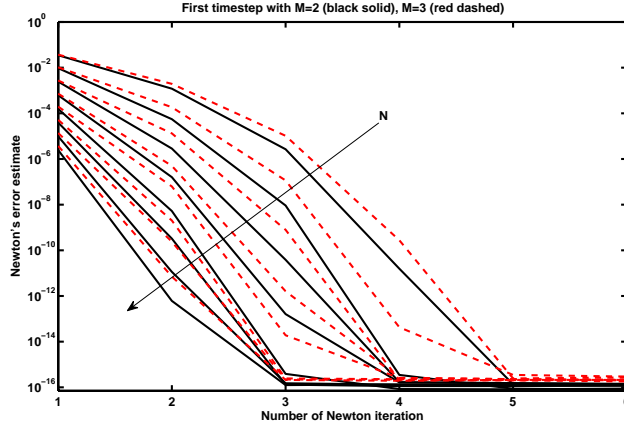


Figure 3: History of the convergence of the Newton iterations during the first timestep. Black solid lines correspond to $m = 2$ and red dashed ones to $m = 3$. We show the results for N ranging from 32 to 4096: the behavior under grid refinement is indicated by the thin arrow.

Figure 1 plots the l_2 errors between the numerical solution at time $t = 20/32$ and the exact solution (26) and shows that the method is first order convergent, as expected for this choice of time stepping procedure and also due to the presence of the singularity in the first derivative of the exact solution. The dashed line is a reference slope for first order schemes. We observe that the convergence is not significantly affected by the parameter m .

Figure 2 plots the number of Newton iterations employed by the algorithm during the integration from $t = 0$ to $t = 20/32$. We plot in black average (circles), minimum and maximum (solid lines) number of Newton iterations per timestep for $m = 2$. For higher values of m we plot only the average (blue symbols). It is worthwhile to note that increasing the number N of points in the grid, causes a slight decrease in the number of iterations for the $m = 2$ case. On the other hand, for higher values of m , when the discontinuity becomes stronger, this decrease is not observed, but the number of Newton iterations remains nevertheless very reasonable.

Next we verify the convergence of the Newton's method (7). In Figure 3 we plot the Newton's error estimate $\|\vec{U}^{1,k+1} - \vec{U}^{1,k}\|/\|\vec{U}^{1,k}\|$ obtained when computing the first timestep \vec{U}^1 . We compare different number of grid points ($N = 32, 64, \dots, 4096$) as indicated by the thin arrow and two values for the exponent m appearing in (25).

We emphasize that as prescribed in Proposition 2.2 the choice of $\Delta t = h$ is acceptable for the convergence both of the global numerical scheme and for the convergence of the Newton procedure.

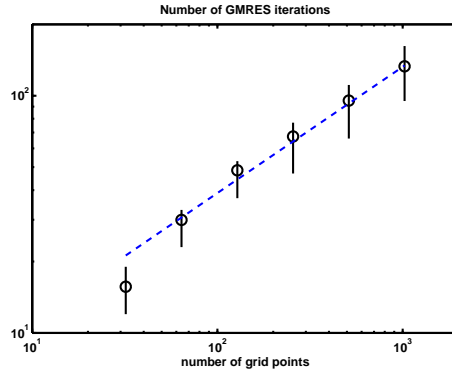


Figure 4: Average, minimum and maximum number of GMRES iterations performed during the integration until final time. The dashed line is the least square fit.

4.2 Solution of the linear system

This part is devoted to computational proposals for the solution of a linear system where the coefficient matrix is the Jacobian in (6), as required at every step of the Newton procedure. As already stressed in Subsection 3.1, the matrix is (weakly) non-symmetric so we start by considering the use of preconditioned GMRES. For all the tests, we set $m = 2$, final time $t = 20/32$, $\Delta t = h$, and we let N be equal to 32, 64, \dots , 1024 for checking the optimality or the proposed best solvers.

4.2.1 GMRES

In Figure 4 we plot the average (circles), minimum and maximum (vertical lines) number of GMRES iterations performed during the integration until the final time ($\Delta t = h$ at different spatial resolutions). A least square fit shows that the number of iterations grows as $N^{0.5320}$. This fact is in complete accordance with the spectral analysis given in Subsection 3.1, since the conditioning grows linearly as N and the eigenvector matrix is almost unitary since the non-symmetric perturbation is negligible also in the subspace of eigenvectors of the symmetric part associated with the smallest eigenvalues. Therefore the GMRES theory of convergence estimates [G97, Sa96] that the number of iteration should be of the order of the square root of the conditioning and this is what we observe in practice.

As already observed, in Subsection 3.1 we have have proven that $Y_N(\cdot)$ is negligible with respect to the symmetric positive definite term $X_N(\cdot) = L_{D(\cdot)} + hI_N$. Accordingly, it is natural to choose $X_N(\cdot)$ as preconditioner for any Krylov based technique. Indeed there is a strong spectral clustering of the preconditioned matrix at 1 and so we expect a number of iterations not depending on the size N of the matrix: this fact is observed in practice and indeed the iteration count

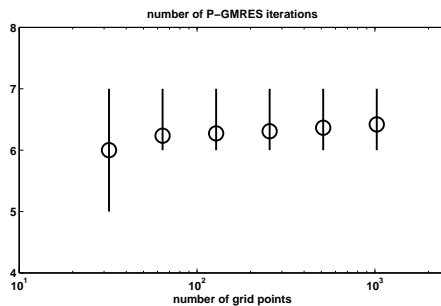


Figure 5: Average, minimum and maximum number of GMRES iterations, with preconditioner X_N , performed during the integration until final time.

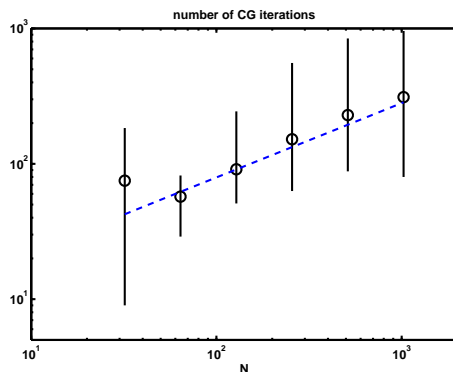


Figure 6: Average, minimum and maximum number of CG iterations performed during the integration until final time. The dashed line is the least square fit.

of the preconditioned GMRES is almost constant, with average value equal to 6 iterations (see Figure 5).

At this point we are left with the problem of solving efficiently a generic linear system with coefficient matrix $X_N(\cdot)$, where the latter is a regularized version of a weighted Laplacian that is a shift of $-L_{D(\cdot)}$ by $h^2/\Delta t = h$ times the identity. A standard V-cycle is in fact optimally convergent since the matrix is slightly better than a standard Laplacian. Indeed, as already remarked, since the non-symmetric part is negligible, we can try directly the solution of the whole system by using techniques such as the preconditioned conjugate gradient (PCG) or the multigrid method which in theory should suffer from the loss of symmetry in the linear system.

4.2.2 CG

In Figure 6 we plot the average (circles), minimum and maximum (vertical lines) number of CG iterations performed during the integration until final time with

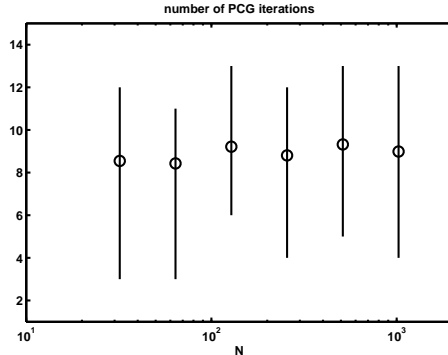


Figure 7: Average, minimum and maximum number of PCG iterations, with preconditioner $X_N(\cdot)$, performed during the integration until final time.

$\Delta t = h$ at different spatial resolutions. A least square fit shows that the number of iterations grows as $N^{0.5491}$. As previously observed in connection with the GMRES method, the number of iterations is again essentially proportional to \sqrt{N} .

However, the number of iterations for fine grids is a lot higher than the ones with GMRES (up to 950 instead of 160 with a grid of 1024 points) so the latter has to be preferred.

In a similar way, we choose $X_N(\cdot)$ as preconditioner in the preconditioned CG method. Results are shown in Figure 7. The number of iterations is again essentially constant with respect to N , but also in the preconditioned version, the GMRES is slightly better since the number of preconditioned CG iterations, 8 or 9, is higher than the number of PGMRES iterations which was equal to 6. Furthermore we have a higher variance in the number of iterations, due to the weak non-symmetry of whole matrix.

4.2.3 MGM

By making use of the positive definiteness of the real part of the matrix, we can propose the MGM defined and discussed in Section 3.2 as iterative solver. We employ the Galerkin approach with $(P_{i+1}^i)^H$ as linear interpolation, so that the projector operator is the one used in geometric multigrid for the Laplacian. We apply a single recursive call that is we remain with the classical V -cycle procedure. As smoother, we consider a unique Jacobi step with damping factor equal to $2/3$. As a result, we observe mesh independent behavior with 10 or 11 iterations (see Figure 8). We have also tried other more sophisticated multi-iterative approaches by adding one step of post-smoother with Gauss-Seidel and standard Jacobi: the number of iterations drops to 6, but the cost per iteration is close to double so that we do not observe a real advantage. The use of one step of CG or one step of GMRES as post-smoother is not better while one step of preconditioned GMRES with preconditioner equal to $X_N(\cdot) =$

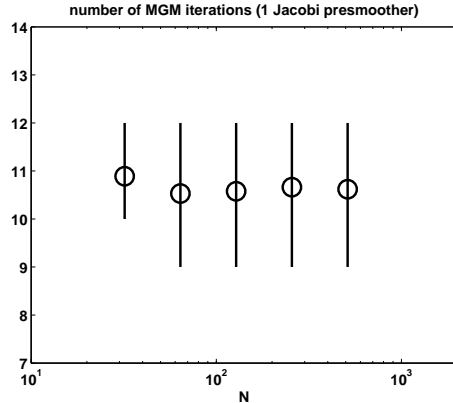


Figure 8: Average, minimum and maximum number of MGM iterations performed during the integration until final time.

$I_N - \frac{\Delta t^2}{h} L_{D(\cdot)}$ reduces substantially the number of iterations, but not enough compared with the cost of the solver needed for handling a generic system with the preconditioner as coefficient matrix.

4.2.4 Krylov methods with MGM as preconditioner

The previous experiments confirm that the MGM is an excellent solver for our linear system. For increasing the robustness, often this method is also applied as preconditioner in a Krylov method instead of employing it as a solver. In other words, as preconditioning step, we just perform a single cycle of the proposed MGM with the same coefficient matrix and where the datum is the residual vector at the current iteration.

With the use of such very cheap MGM preconditioning, the GMRES converges within 4 or 5 iterations independently of the size of the involved matrices (see Figure 9).

Analogously, the application of the very same MGM preconditioning in the preconditioned CG method leads to a convergence within 7 or 8 iterations, again independently of the system sizes (see Figure 10).

In conclusion, it seems that the latter proposal in connection with GMRES has to be preferred, taking into account the simplicity, the robustness (less variance in the iteration count), and the number of iterations. Indeed, due to the small iteration count, also the number of vectors that have to be stored in the GMRES process is absolutely reasonable.

5 Sample application: marble sulfation

Here we consider the model for the marble sulfation problem described in [ADDN04]. We describe the main features of the model only briefly, referring

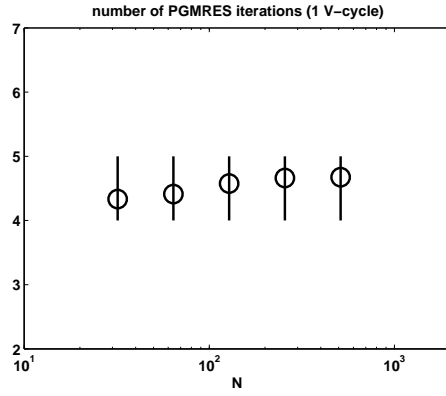


Figure 9: Average, minimum and maximum number of GMRES iterations, with preconditioner given by one step of the MGM, performed during the integration until final time.

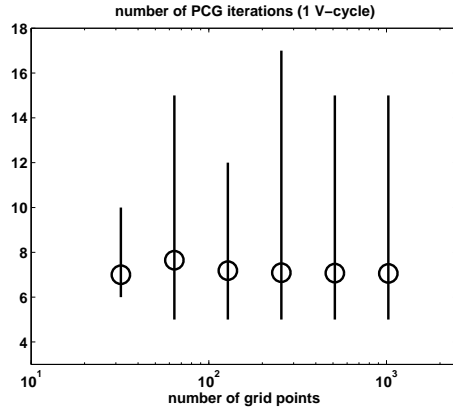
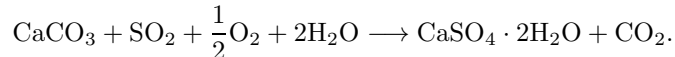


Figure 10: Average, minimum and maximum number of PCG iterations, with preconditioner MGM, performed during the integration until final time.

the reader to the original paper for the details and more comprehensive study of the properties of the solutions. [ADDN04] consider the (simplified) chemical reaction



To account for the transformation of CaCO_3 in the marble stone into gypsum $\text{CaSO}_4 \cdot 2\text{H}_2\text{O}$ triggered in a moist atmosphere by the availability of SO_2 at the marble surface and inside the pores of the stone. The two main variables of the model are $c(t, x)$ denoting the local concentration of calcium carbonate and $s(t, x)$ the local concentration of SO_2 . As the reaction proceeds, the calcium carbonate concentration is reduced from the initial value c_0 , as CaCO_3 is progressively replaced by gypsum. Denoting φ_0 and φ_g the porosity of the pristine marble and of the gypsum, the model assumes that the porosity of the intermediate state is well approximated by linear interpolation

$$\varphi(c) = \varphi_g + (\varphi_0 - \varphi_g)\frac{c}{c_0} = \alpha c + \beta.$$

The constants α and β depend on the porosity of the material involved. The model considered in [ADDN04] is described by the following system of PDEs:

$$\begin{cases} \frac{\partial \varphi(c)s}{\partial t} &= -\frac{A}{m_c}\varphi(c)sc + d\nabla \cdot (\varphi(c)\nabla s), \\ \frac{\partial c}{\partial t} &= -\frac{A}{m_s}\varphi(c)sc. \end{cases} \quad (27)$$

The spatial domain $x \in \Omega$ in which (27) is set represents a portion of the marble stone for which at least a portion of the boundary $\partial\Omega$ is in contact with the polluted atmosphere. In particular $\partial\Omega$ is in general split into two parts: a portion that represents the outer surface of the marble sample, in contact with the air and the complementary part that separates the portion of the marble object of the simulation and the rest of the monument. Examples of one and two-dimensional such domains are shown in Figure 11. Boundary conditions are set by imposing the value of s on the outer boundary and by imposing free-flow conditions for s on the inner boundary. In the one-dimensional setting that we consider in this paper, we take $x \in \Omega = [0, 1]$ where $x = 0$ corresponds to the outer boundary of the marble stone, in contact with the polluted air, and $x = 1$ the inner side. The boundary conditions are illustrated in Figure 11: they are of Dirichlet type, imposing $s(0, t)$ on the outer boundary and of free-flow type $\frac{\partial s}{\partial x}(1, t) = 0$ on the inner side.

The parameters m_s and m_c are fixed by the physical properties of the species involved in the reaction and make sure that the mass balance is fulfilled. On the other hand A represents the reaction rate and it depends (among other things) on the moisture of the air and on the temperature. [ADDN04] describes its central role in the analysis of the solutions of the model equations. In particular, if $u(t, x)$ is a solution of (27) for a given value of A , then $\tilde{u}(t, x) = u(t/A^2, x/A)$ is a solution of (27) for $A = 1$. This observation on one hand plays a fundamental

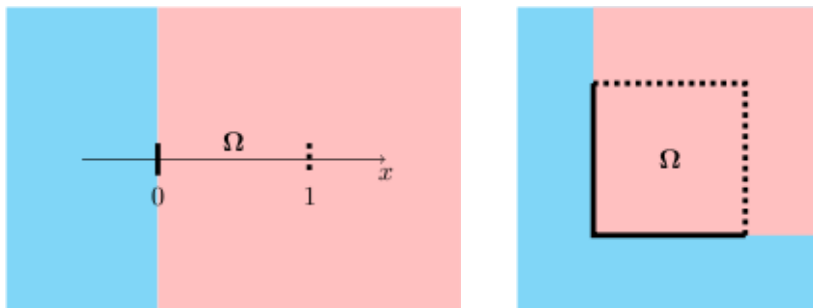


Figure 11: Sample domains Ω for problem (27) are shown for the 1D setting (left) and 2D setting (right). The pink area represents the marble stone, while the cyan area is air. The boundary is drawn with a solid line where Dirichlet boundary conditions are applied and with a dotted line where free-flow boundary conditions are imposed.

role in establishing the long-time asymptotics of the solution and would allow to perform the simulations with $A = 1$ and then rescale the numerical solutions appropriately to take the reaction rate into account. However, because of its role as fundamental physical parameter of the model, here we prefer to keep A explicitly into the equations and perform simulations seeking numerical solution of the model in the form (27). Moreover this is beneficial in view of the more complete model including a non-constant A has been described in [AFNT07].

We consider, as in [ADDN04] $\alpha = 0.01$, $\beta = 0.1$, $d = 1$, $m_s = 64.06$, $m_c = 100.09$ and use $h = 1/64$ or $h = 1/128$ while varying A from 1 to 10^5 .

5.1 Discretization

We consider a discretization based on the Crandall-Liggett formula in time and finite differences in space. We denote $x_\xi = 0 + \xi h \in \Omega$. Approximating the elliptic operator along the same lines as in (3), we consider the second order finite difference formula

$$\partial_x(\varphi(c)\partial_x s)|_{x_j} = \frac{\varphi(c(x_{j+1/2}))(s(x_{j+1}) - s(x_j))}{h^2} - \quad (28)$$

$$- \frac{\varphi(c(x_{j-1/2}))(s(x_j) - s(x_{j-1}))}{h^2}. \quad (29)$$

This in turn suggests that we employ two staggered grids in the domain Ω : the grid x_j ($j \in \mathbb{N}$) with the unknowns s_j^n for $s(t^n, x_j)$ and the grid $x_{j+1/2}$ ($j \in \mathbb{N}$) with the unknowns $c_{j+1/2}^n$ for $c(t^n, x_{j+1/2})$. For short, we also denote $\varphi_{j+1/2}^n = \varphi(c_{j+1/2}^n)$.

Following (2), the scheme that we propose computes s_j^n and $c_{j+1/2}^n$ solving

the nonlinear system of equations:

$$\begin{cases} 0 = \mathbf{F}_j^{(s)}(s, c) = & \frac{\varphi_{j+1/2}^n + \varphi_{j-1/2}^n}{2} s_j^n - \frac{\varphi_{j+1/2}^{n-1} + \varphi_{j-1/2}^{n-1}}{2} s_j^{n-1} \\ & + \Delta t \frac{A}{m_c} \frac{\varphi_{j+1/2}^n c_{j+1/2}^n + \varphi_{j-1/2}^n c_{j-1/2}^n}{2} s_j^n \\ & + d \frac{\Delta t}{h^2} \left[-\varphi_{j-1/2}^n s_{j-1}^n + (\varphi_{j-1/2}^n + \varphi_{j+1/2}^n) s_j^n - \varphi_{j+1/2}^n s_{j+1}^n \right] \\ 0 = \mathbf{F}_{j+1/2}^{(c)}(s, c) = & c_{j+1/2}^n - c_{j+1/2}^{n-1} + \Delta t \frac{A}{m_s} \varphi_{j+1/2}^n c_{j+1/2}^n \left(\frac{s_{j+1}^n + s_j^n}{2} \right) \end{cases} \quad (30)$$

The 2 staggered grids are a sort of finite difference analogue of the approximation with $P1$ (for $s(x)$) and $P0$ (for $c(x)$) conforming finite elements considered in [ADDN04]. The results obtained here on preconditioning should also be applicable with little modifications in that case too.

The Crandall-Liggett formula gives an unconditionally stable scheme. Following the results previously established, in order to solve the nonlinear problem (30) we set up Newton iterations. To this end we need the Jacobian matrix, whose entries are:

$$\begin{aligned} \frac{\partial \mathbf{F}_j^{(s)}}{\partial s_k} &= \frac{\varphi_{j+1/2} + \varphi_{j-1/2}}{2} \delta_{jk} + \Delta t \frac{A}{m_c} \frac{\varphi_{j+1/2} c_{j+1/2} + \varphi_{j-1/2} c_{j-1/2}}{2} \delta_{jk} \\ &+ d \frac{\Delta t}{h^2} \left[-\varphi_{j-1/2} \delta_{k,j-1} + (\varphi_{j-1/2} + \varphi_{j+1/2}) \delta_{k,j} - \varphi_{j+1/2} \delta_{k,j+1} \right], \\ \frac{\partial \mathbf{F}_j^{(s)}}{\partial c_{k+1/2}} &= \frac{\varphi'_{j+1/2} s_j \delta_{kj} + \varphi'_{j-1/2} s_j \delta_{k+1,j}}{2} \\ &+ \Delta t \frac{A}{m_c} \frac{(\varphi'_{j+1/2} c_{j+1/2} + \varphi_{j+1/2}) \delta_{jk} + (\varphi'_{j-1/2} c_{j-1/2} + \varphi_{j-1/2}) \delta_{j,k+1}}{2} \\ &+ d \frac{\Delta t}{h^2} \left[\varphi'_{j-1/2} (s_j - s_{j-1}) \delta_{j,k+1} - \varphi'_{j+1/2} (s_{j+1} - s_j) \delta_{j,k} \right], \\ \frac{\partial \mathbf{F}_{j+1/2}^{(c)}}{\partial s_k} &= \Delta t \frac{A}{m_s} \varphi_{j+1/2} c_{j+1/2} \frac{\delta_{j,k-1} + \delta_{jk}}{2}, \\ \frac{\partial \mathbf{F}_{j+1/2}^{(c)}}{\partial c_{k+1/2}} &= \left[1 + \Delta t \frac{A}{m_s} (\varphi'_{j+1/2} c_{j+1/2} + \varphi_{j+1/2}) \frac{s_{j+1} + s_j}{2} \right] \delta_{jk}. \end{aligned} \quad (31)$$

Boundary conditions are imposed considering $j = 1, 2, \dots, N$ in (30) and assuming at all time steps a given value for s_0 (Dirichlet boundary condition at $x = 0$) and that $s_{N+1} = s_{N-1}$ (homogeneous Neumann boundary condition at $x = 1$). Thus the expressions of $\mathbf{F}_1^{(s)}$ and $\mathbf{F}_N^{(s)}$ are modified accordingly with respect to those in (30), together with the correspondent elements in the Jacobian (31). The $2N$ unknowns are collected in a vector U with the ordering $U = [s_1, s_2, \dots, s_N, c_{1/2}, \dots, c_{N-1/2}]^T$. The corresponding sparsity structure of the Jacobian matrix is illustrated in Figure 12. For the implementation it is easier to define the ‘‘porous concentration’’ and set the Dirichlet boundary

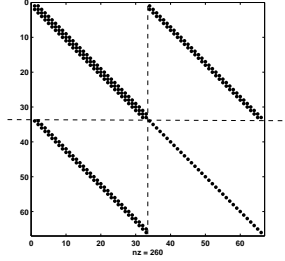


Figure 12: Sparsity structure of the Jacobian matrix (31).

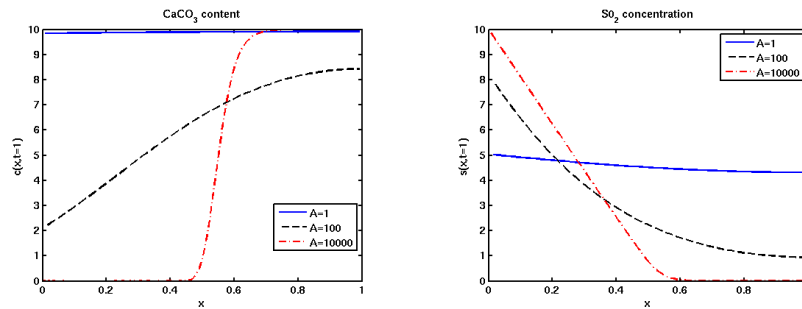


Figure 13: For different values of A , marble content and SO_2 concentration inside the stone predicted by the model (27) for $t = 1$.

condition as $\varphi_{j-1/2}s_j|_{j=0} = \rho_{s_0} = 1$.

5.2 Simulations and performance of the algorithm

In Figure 13 we plot some typical curves obtained from the simulations with the model (27). Note that for bigger values A , the reaction is faster and a boundary layer appears. For $A = 10^4$, Figure 14 shows the temporal evolution of the two main variables: while SO_2 penetrates deeper and deeper into the stone (right), calcium carbonates is substituted by the more porous gypsum in a narrow spatial band where the curve $c(t, x)$ presents a boundary layer. Once formed, this transition region travels towards the interior of the stone (left). The self-similarity of the solutions of (27) under rescaling of the temporal and spatial variables mentioned at the beginning of Section 5 implies that the boundary layer observed for $A = 10^4$ will also appear for lower values of A , if the solutions were sought for a larger temporal and spatial domain.

Newton iterations In Figure 15 we plot the average, minimum and maximum number of Newton iterations used by the numerical method to solve the nonlinear equation (30) at each timestep.

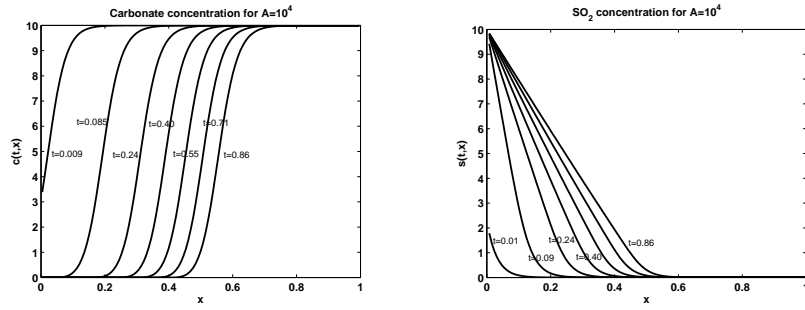


Figure 14: Temporal evolution of the calcium carbonate and sulfate concentration predicted by the model (27) with $A = 10^4$.

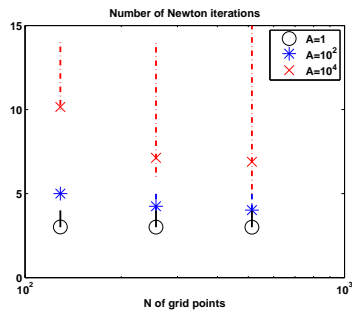


Figure 15: Number (average, min and max) of Newton iterates per timestep.

For $A = 1$ (black circles) we note that the number of iterations is almost constant when the number of grid points is increased. Furthermore, for a given number of points employed in the discretization, the number of Newton iterations increases very moderately even when A is increased by several orders of magnitude: e.g. for $N = 128$ we need an average of 3 Newton iterations per timestep for $A = 1$, 5 for $A = 100$ (blue stars), and 10 for $A = 10000$ (red crosses). Finally we point out that for higher values of N , the number of Newton iterations decreases slightly since the grid becomes able to resolve better the boundary layer.

Solving the linear system Finally we study the number of linear iterations performed inside each nonlinear Newton step, in order to solve the linear system with matrix (31), which we recall having the block structure

$$J = \begin{bmatrix} F_s^s & F_c^s \\ F_s^c & F_c^c \end{bmatrix} \quad U = \begin{pmatrix} U_s \\ U_c \end{pmatrix}$$

also depicted in Figure 12.

Since J is not symmetric, we employ GMRES as a main Krylov solver. In Figure 16 we plot the average, minimum and maximum number of GMRES iterations needed in the case $A = 1$ and for different values of the number of grid points N . Since the number of iterations scales as $N^{0.5217}$, we studied a suitable preconditioner.

First, observing that F_c^c is diagonal, we take the block upper triangular part of J as a preconditioner P and solve the block triangular system $Py = b$ as

$$y_c = (F_c^c)^{-1}b_c \quad y_s = (F_s^s)^{-1}(b_s - F_c^s y_c)$$

(Here the subscripts s and c denote respectively the upper and lower half of a vector, i.e. those relative to the sulfate and the carbonate degrees of freedom) The second linear system in the previous formula is $N \times N$ with tridiagonal matrix with a structure similar to the matrix X_N studied in Section 2.2. Hence as a first approach we employ MGM to solve it: the left panel of Figure 17 shows the number resulting outer GMRES and inner MGM iterations.

Finally we observe that it is not advantageous to drive the MGM algorithm for the F_s^s system all the way until convergence: instead performing just 1 MGM V-cycle is enough to get an optimal preconditioner, i.e. to render the number of GMRES iterations independent from N (see right panel of Figure 17).

As already observed the method that in practice works in the best way is the GMRES with one step of the simplest V-cycle. We observe an impressive series of good features: minimal average computational cost, minimal number of iterations, minimal variance in the latter number meaning a strong robustness of the procedure.

5.3 Comparison with real data

In [GSNF08] the results of an experiment aimed at assessing the relevance of the sulfation model (27) are reported. Marble samples were exposed to a continuous

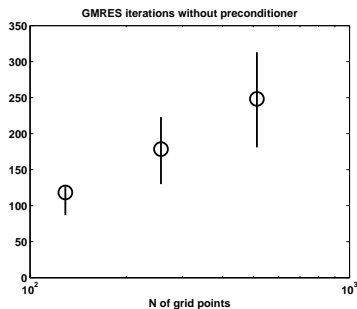


Figure 16: Number (average, min and max) of GMRES iterates per timestep with $A = 1$, for 3 values of N . No preconditioner was used in this test.

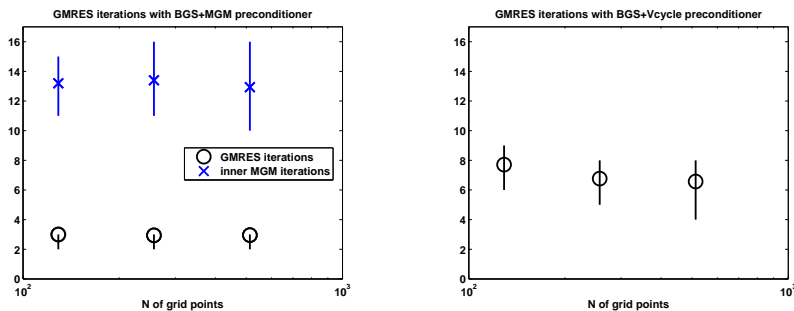


Figure 17: Number (average, min and max) of GMRES iterates per timestep with $A = 1$, for 3 values of N . Block Gauss-Seidel and MGM for the upper left block was used as a preconditioner. In the left panel, blue symbols and lines refer to the number of inner MGM iterations.

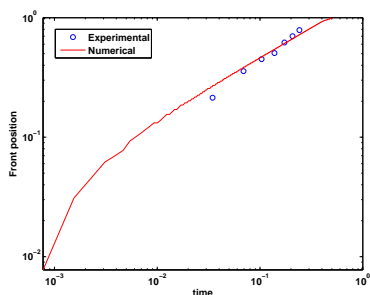


Figure 18: Gypsum-carbonate front position in a sulfation problem: experimental data from [GSNF08] and numerical simulation.

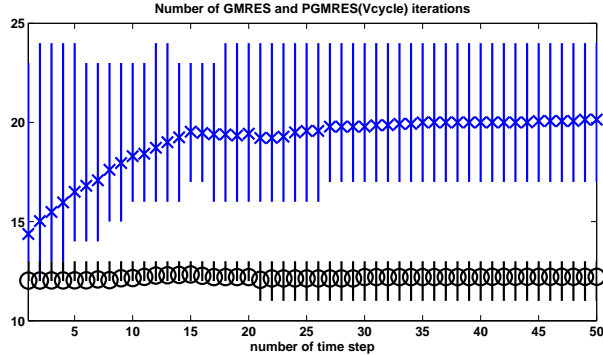


Figure 19: Number of GMRES iterations per Newton step: for each timestep we plot the average, minimum and maximum number of linear iterations. Without preconditioner: blue, crosses. With Vcycle preconditioner: black, circles.

flow of SO_2 inside a purpose built experimental device that guarantees that the one dimensional approximation considered here is satisfied. Using high SO_2 concentration allowed to obtain gypsum crusts of measurable thickness within just a few days. The average values of the crust thickness for values of exposure time from 1 to 7 days are reported in [GSNF08].

Unfortunately no information is given in [GSNF08] on the type of marble used (porosity, initial carbonate concentration, etc), nor on the standard deviation of the experimental values. The knowledge of these data in a real situation would allow to choose accordingly the A , c_0 , α , β coefficients. Thus here we just want to prove that it is possible to fit the experimental data with the output of a suitable numerical simulations. In particular we choose $A = 10^5$ and $c_0 = 1$.

In order to perform the comparison, we extracted the information on the front position from the numerical solutions $c_{j+1/2}^n$ by identifying the gypsum-carbonate front with the point with steepest gradient of $c(t^n, x)$. Figure 18 shows a comparison of the numerical front position (red solid line) and the experimental data (blue circles). Note that the step-like behavior of the numerical front that is apparent in some regions of the graph is due to the finite spatial resolution of the simulation ($h = 1/128$).

Note also that the long time behavior of the front position $x_{\text{front}} \sim \sqrt{t}$ which is predicted by the asymptotic analysis of [GN07] is well confirmed by the data in Figure 18.

5.4 Sample application in 2D

In this section we present a numerical simulation of equations (27) in the two dimensional setting of figure 11. We consider again two staggered quadrangular regular grids in $\Omega = [0, 1] \times [0, 1]$. When using N points per direction, we denote $x_\xi = \xi/N$ and $y_\xi = \xi/N$. We generalize the construction of Section 5.1 consid-

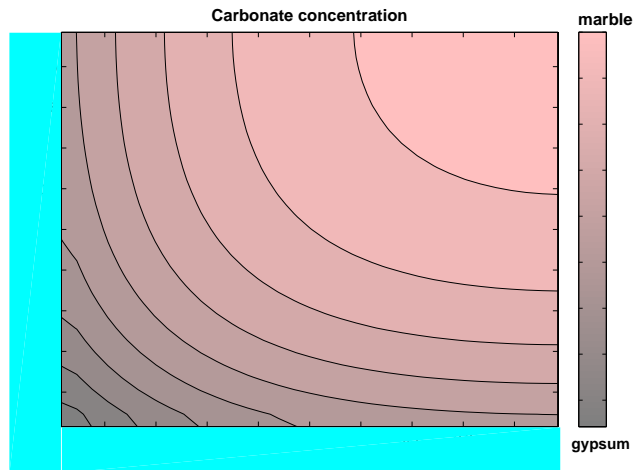


Figure 20: Simulation of marble sulfation in two dimensions.

ering two staggered grids: the set of points $\{(x_i, y_j)\}_{i,j=0}^N$ carrying the values $s_{i,j}$ of the SO_2 concentration field $s(x, y)$ and the set $\{(x_{i+1/2}, y_{j+1/2})\}_{i,j=1}^N$ carrying the values $c_{i+1/2, j+1/2}$ of the calcium carbonate concentration field. The discretization of the elliptic operator is then generalized in the usual way to the two dimensional setting, and the new form of the fixed point problem (30) and its laplacian (31) are derived. The numerical scheme now requires, at each timestep, the solution of a system of $2N^2$ nonlinear equations. Using again the Newton method, at each iteration we need to solve a sparse linear system with a matrix of dimension $2N^2 \times 2N^2$. This can be achieved by using GMRES as main Krylov solver with specialized structured preconditioners as in the one dimensional case.

Here we consider only the best preconditioner of those evaluated in the one dimensional setting, namely the upper triangular part of the jacobian matrix, where we perform only 1 V-cycle on the (s, s) block. In Figure 19 we study the effectiveness of this preconditioning technique. On a 32×32 grid, we observe that unpreconditioned GMRES requires an average of 15 to 20 iterations to solve the jacobian linear system in each Newton step, with frequent peaks of 24 iterations (blue crosses in the figure are the average values, blue lines the minimum to maximum range). Moreover the number of iterations is not constant but depends on the timestep. On the contrary the preconditioned method employs always an average of 12 PGMRES iterations, with little variability both within the time step and across the different times (black circles and lines).

In Figure 20 we plot the solution obtained for $A = 10$. We recall the the marble is incontact with the polluted air at the bottom and left boundary (cyan regions), while at the top and right boundary we apply free flow conditions. Both the colour code and the isolines refer to the carbonate concentration in

the stone. We observe a clear deformation of the CaCO_3 field near the corner, clearly indicating that SO_2 , penetrating from both sides, causes an enhanced loss of material: if the gypsum crust were to fall off here, the sharp edge would be chipped off and the shape of the stone would be permanently changed.

This simulation, although performed at low resolution (32×32 grids) and with a moderate value of A , already indicates the relevance of our project of developing accurate numerical simulators for realistic geometries of the domain Ω in two and three dimensions.

6 Conclusions and future developments

The novel contribution of this paper relied in the proposal of a fully implicit numerical method for dealing with the nonlinear PDE, in its convergence and stability analysis, and in the study of the related computational cost. Indeed the nonlinear nature of the underlying mathematical model required the application of a fixed point scheme. We have identified the classical Newton method in which, at every step, the solution of a large, locally structured, linear system has been handled by using specialized iterative or multi-iterative solvers. In particular, we have provided a spectral analysis of the relevant matrices which has been crucial for identifying appropriate preconditioned Krylov methods with efficient V-cycle preconditioners. Numerical experiments for the validation of our multi-facet analysis have complemented this contribution, which is aimed to provide a non-invasive tool for a quantitative forecast of the damage evolution in a given monument.

In particular we considered the application of the abovementioned techniques to the numerical approximation of a mathematical model describing the damage of marble monuments by the sulfation process. The use of our resulting fast integration algorithms allows to exploit the model and its predictive power for the strategy known as *planned conservation*, that is the novel approach that privileges the study and prevention of the damages to delay and optimize the actual restoration works. We showed both one dimensional and two dimensional numerical simulations, using simple domains.

As relevant steps in the future we indicate the following directions:

- We will continue the study of the numerical methods introduced so far with a rigorous analysis of the approximation error.
- We will consider finite element methods for the space discretization in order to deal with more realistic domains in 2D and 3D, that can model a real architectural item with a complicate geometry.
- A natural extension of the numerical treatment for the sulfation problem involves considering the 3-equations model in [AFNT07] and/or a model for a remediation technique, like the one in [CGN⁺] (this will include consolidation models that is systems of the type $u_t = (D(u)(p(u)_x))_x$). As a

long term goal, being able to simulate both the damage and the remediation process with validated mathematical models and numerical methods would allow to perform numerical experiments of restoration works.

References

- [ADDN04] D. Aregba Driollet, F. Diele, and R. Natalini. A mathematical model for the SO_2 aggression to calcium carbonate stones: numerical approximation and asymptotic analysis. *SIAM J. Appl. Math.*, 64(5):1636–1667, 2004.
- [ADS04] A. Aricó, M. Donatelli, and S. Serra-Capizzano. V-cycle optimal convergence for certain (multilevel) structured linear systems. *SIAM J. Matrix Anal. Appl.*, 26(1):186–214, 2004.
- [AFNT07] G. Alì, V. Furuholt, R. Natalini and I. Torcicollo. A mathematical model of sulphite chemical aggression of limestones with high permeability. I. Modeling and qualitative analysis. *Transp. Porous Media*, 69(1):109–122, 2007.
- [AL86] O. Axelsson and G. Lindskog. The rate of convergence of the preconditioned conjugate gradient method. *Numer. Math.*, 52:499–523, 1986.
- [BS07] B. Beckermann and S. Serra-Capizzano. On the asymptotic spectrum of Finite Elements matrices. *SIAM J. Numer. Anal.*, 45(2):746–769, 2007.
- [BBR79] A.E. Berger, H. Brézis, and J.C.W. Rogers. A numerical method for solving the problem $u_t - \Delta f(u) = 0$. *RAIRO Anal. Numér.*, 13(4):297–312, 1979.
- [BGST05] D. Bertaccini, G. Golub, C. Tablino Possio, and S. Serra-Capizzano. Preconditioned HSS methods for the solution of non-Hermitian positive definite linear systems and applications to the discrete convection-diffusion equation. *Numer. Math.*, 99(3):441–484, 2005.
- [Bh97] R. Bhatia. *Matrix Analysis*. Springer Verlag, New York, 1997.
- [BLTR00] R. Bugini, M. Laurenzi Tabasso, and M. Realini. Rate of formation of black crusts on marble. a case study. *J. Cultural Heritage*, 1:111–116, 2000.
- [BP72] H. Brézis and A. Pazy. Convergence and approximation of semi-groups of nonlinear operators in Banach spaces. *J. Functional Analysis*, 9:63–74, 1972.

- [CGN⁺] F. Clarelli, C. Giavarini, R. Natalini, C. Nitsch, and M.L. Santarelli. Mathematical models for the consolidation processes in stones. In J. Delgado Rodrigues, editor, *Proc. of "International Symposium: Stone Consolidation in Cultural Heritage - research and practice"*. Lisbona, May 2008. to appear.
- [CL71] M.G. Crandall and T.M. Liggett. Generation of semi-groups of non-linear transformations on general Banach spaces. *Amer. J. Math.*, 93:265–298, 1971.
- [CNPS07] F. Cavalli, G. Naldi, G. Puppo, and M. Semplice. High-order relaxation schemes for nonlinear degenerate diffusion problems. *SIAM J. Numer. Anal.*, 45(5):2098–2119 (electronic), 2007.
- [GKAC89] K.L. Gauri, N.P. Kulshreshtha, A.R. Punuru, and A.N. Chowdhury. Rate of decay of marble in laboratory and outdoor exposure. *J. Mater. Civil Eng.*, 1:73–85, 1989.
- [GSNF08] C. Giavarini, M.L. Santarelli, R. Natalini, and F. Freddi. A nonlinear model of sulphation of porous stones: numerical simulations and preliminary laboratory assessments. *J. Cultural Heritage*, 9:14–22, 2008.
- [GS07] L. Golinskii and S. Serra-Capizzano. The asymptotic properties of the spectrum of non symmetrically perturbed Jacobi matrix sequences. *J. Approx. Th.*, 144(1): 84–102, 2007.
- [GV83] G. Golub and C. Van Loan. *Matrix Computations*. The Johns Hopkins University Press, Baltimore, 1983.
- [G97] A. Greenbaum. *Iterative methods for solving linear systems*. SIAM publ., Philadelphia, 1997.
- [GN05] F.R. Guarguaglini and R. Natalini. Global existence of solutions to a nonlinear model of sulphation phenomena in calcium carbonate stones. *Nonlinear Anal. Real World Appl.*, 6(3):477–494, 2005.
- [GN07] F.R. Guarguaglini and R. Natalini. Fast reaction limit and large time behavior of solutions to a nonlinear model of sulphation phenomena. *Comm. Partial Differential Equations*, 32(1-3):163–189, 2007.
- [H85] W. Hackbusch. *Multigrid Methods and Applications*. Springer Verlag, Berlin, Germany, 1985.
- [Hay83] F.H. Hayne. Deterioration of marble. *Durability Build. Mater.*, 1:241–254, 1982/83.
- [Lip89] W.T. Lipfert. Atmospheric damage to calcareous stones: comparison and reconciliation of recent experimental findings. *Atmos. Environ.*, 23:415–429, 1989.

- [MNV87] E. Magenes, R.H. Nochetto, and C. Verdi. Energy error estimates for a linear scheme to approximate nonlinear parabolic problems. *RAIRO Modél. Math. Anal. Numér.*, 21(4):655–678, 1987.
- [OR70] J.M. Ortega and W.C. Rheinboldt. *Iterative Solutions of Nonlinear Equations in Several Variables*. Academic Press, New York, 1970.
- [RS87] J.W. Ruge and K. Stüben. *Algebraic Multigrid*. Frontiers in Applied Mathematics: Multigrid Methods, S. McCormick Ed. SIAM, Philadelphia (PA): 73-130, 1987.
- [Sa96] Y. Saad. *Iterative Methods for Sparse Linear Systems*. PWS, Boston, 1996.
- [S93] S. Serra-Capizzano. Multi-iterative methods. *Comput. Math. Appl.*, 26(4):65–87, 1993.
- [S99] S. Serra-Capizzano. The rate of convergence of Toeplitz based PCG methods for second order nonlinear boundary value problems. *Numer. Math.*, 81(3):461–495, 1999.
- [S02] S. Serra-Capizzano. Convergence analysis of Two-Grid methods for elliptic Toeplitz and PDEs matrix-sequences. *Numer. Math.*, 92(3):433–465, 2002.
- [S02] S. Serra-Capizzano. GLT sequences as a Generalized Fourier Analysis and applications. *Linear Algebra Appl.*, 419(1):180–233, 2006.
- [ST04] S. Serra-Capizzano and C. Tablino Possio. Multigrid methods for multilevel circulant matrices. *SIAM J. Sci. Comput.*, 26(1):55–85, 2004.
- [T98] P. Tilli. Locally Toeplitz matrices: spectral theory and applications. *Linear Algebra Appl.*, 278:91–120, 1998.
- [TOS01] U. Trottenberg, C.W. Oosterlee, and A. Schüller. *Multigrid*. Academic Press, London, 2001.
- [V62] R.S. Varga. *Matrix Iterative Analysis*. Prentice/Hall, New York, 1962
- [VV01] H.A. van der Vorst and C. Vuik. The superlinear convergence behavior of GMRES. *J. Comput. Appl. Math.*, 48:327–341, 1993.